AD-A221 329

Office of the Chief of Naval Research
Contract N00014-89-J-1276
Technical Report No. UWA/DME/TR-90/66

AXIAL CRACK PROPAGATION AND ARREST IN PRESSURIZED FUSELAGE

Makoto Kosai and Albert S. Kobayashi

DTIC
ELECTE
MAY 10 1990
S D
E

April 1990

The research reported in this technical report was made possible through support extended to the Department of Mechanical Engineering, University of Washington, by the Office of Naval Research under Contract N00014-89-J-1276. Reproduction in whole or in part is permitted for any purpose of the United States Government.

Department of Mechanical Engineering
College of Engineering
University of Washington

DISTRIBUTION STATEMENT A
Approved for public release;
Distribution Unlimited

Axial Crack Propagation And Arrest In Pressurized Fuselage

M. KOSAI AND A. S. KOBAYASHI

Department of Mechanical Engineering
University of Washington
Seattle, Washington 98195
USA

Summary

The rapid crack propagation, crack curving and arrest mechanisms associated with a pressurized, thin-walled ductile steel tubes are used to develop a model of axial rupture of an aircraft fuselage. This model is used to replicate axial crack propagation along a line of multi-site damage (MSD) and crack curving and arrest near a tear strap of an idealized fuselage.

Introduction

Static linear elastic fracture mechanics (LEFM) has been used to predict a monotonically increasing stress intensity factor with increasing crack length of an axial crack in a pressurized pipe [1,2] as well as to model dynamic crack branching in a pressurized steel pipe [3]. Plasticity effect has also been incorporated to this LEFM analysis using semi-empirical adjustments [4,5], or by kinematic modelling of the yielded pipe [6]. Many of these analyses, however, do not consider the dynamic effects generated by the propagating axial crack as well as the influence of the large plastic deformation of the crack flaps.

Under the sponsorship of the US Department of Transportation (DOT), one of the author and his colleagues studied axial crack propagation, curving and arrest in a small scale model of a line pipe [7,8]. These experimental results were then used to modify a numerical model, which was previously developed for analyzing bursting thick-walled steam pipes. This study showed that the main driving force of the axial crack in a bursting pipe was the gas pressure acting on the crack flaps which literally tore the pipe apart. It was also found that the axial stretch of the crack flap, not only served as an energy dissipation mechanism, but also imposed an axial tensile stress, which is larger than the hoop stress, as much as five pipe diameters ahead of the crack tip thus leading to crack curving and crack arrest.

While an aircraft fuselage is an infinitely more complicated structure than a monolithic line pipe, the crack propagation, curving and arrest mechanisms of the latter could be of use in a postmortem analysis of a fuselage failure as well as for estimating the crack arrest capability of a tear strap. In the following, a brief

review of the cogent results generated in the DOT pipe fracture study as well as the crack curving and crack branching criteria, which were developed under a Office Naval Research (ONR), contract are presented. These results are then used to assess the crack arrest capability of a hypothetical fuselage with tear straps.

Analysis of Axial Rupture of Subsize Gas Transmission Lines

The experimental phase of the DOT studies consisted of measuring the dynamic depressurization rate, crack extension rate, static and the dynamic axial and circumferential strains along the axial crack in a 2-in. diameter, schedule 10, carbon steel pipe. These pipes were pressurized to approximately 80 percent of the yield strength in hoop stress in a series of static and dynamic pipe rupture experiments. The test section of the pipe was pre-grooved to a depth of approximately 20 percent of the pipe wall thickness to simulate a locally embrittled zone for continuous and controlled axial crack propagation in the ductile pipe wall. Such grooving simulated multi-site damage (MSD) in a fuselage. The grooves were carefully machined to avoid local elevation of the ultimate strength of the pipe wall material due to strain hardening, and thus the pipe wall fractured with a 100% shear lip. The propagating crack always arrested upon entering the ungrooved section, which simulated the fuselage section with a tear strap of the pressurized pipe. The rupturing profiles, i.e., the pipe flap motions, were recorded by a high-speed framing camera. Figure 1 shows typical sequential photographs of a rupturing pipe where the crack bifucated upon entering the ungrooved section of the pipe.

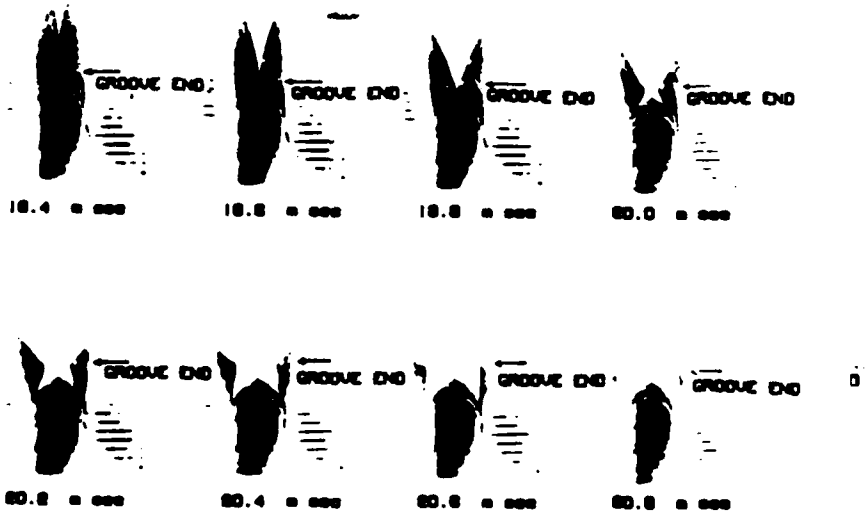

Fig. 1. Axial crack bifucation and arrest in a pressurized steel pipe

A special software for processing the high-speed photographic records and for determining the crack opening displacements (COD) and axial straining along the crack flaps was developed. This data was used to compute the crack tip opening angle (CTOA). The static and dynamic crack opening shapes and CTOA's were

similar and the CTOA remained constant over a crack velocity range of 600 to 1000 fps but varied with the groove depth. When the groove depth was decreased to simulate a tougher pipe material, the CTOA increased and the crack velocity decreased.

Records of the strain gage rosettes, which were placed along the crack path in the dynamic pipe rupture tests, showed that the maximum strain exceeded the yield strain and changed from the circumferential to the axial directions approximately 5 to 9 pipe diameters ahead of the propagating crack tip, as shown in Figures 2 and 3. These results indicated that a long and narrow axial-stretch zone preceded the propagating crack tip. This large axial strain, which is much larger than those reported previously, is consistent with the observations of Shoemaker et al. [9] and Urednicek [10]. The narrow axial-stretch zone is also the essential feature of the thin shell model of a bursting pipe by Freund et al. [11] who used this model to predict crack kinking at arrest due to a mechanical crack arrester [12].

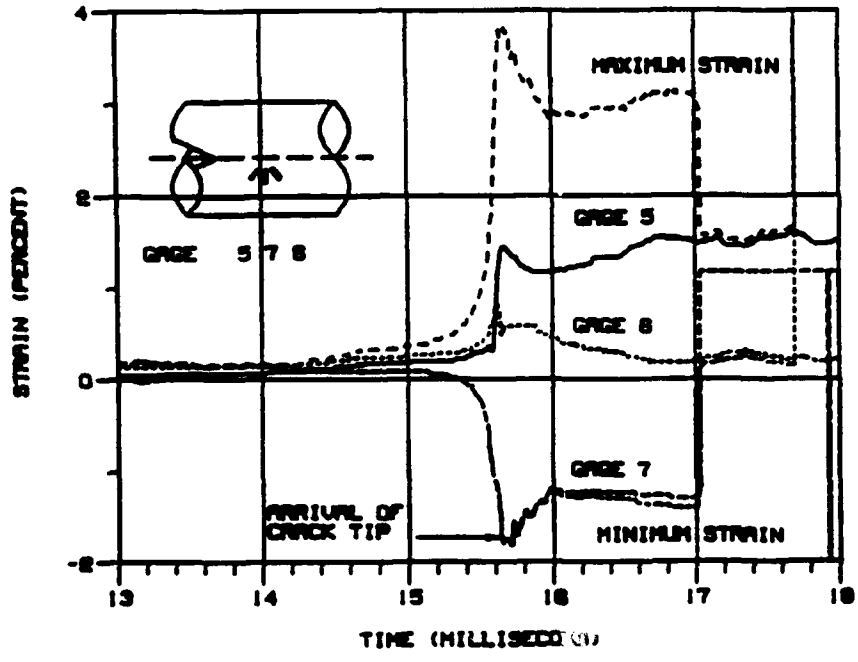

Fig. 2. Strain rosette readings adjacent to a propagating axial crack in a pressurized steel pipe

Accession For	
NTIS GRA&I	☒
DTIC TAB	☐
Unannounced	☐
Justification	
By	
Distribution/	
Availability Codes	
Dist	Avail and/or Special
A-1	

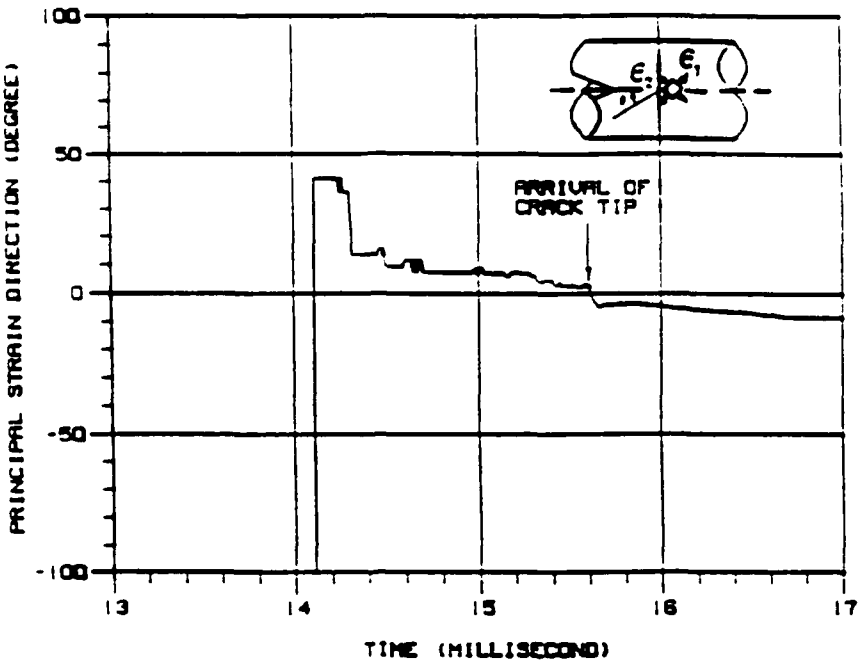

Fig. 3. Variation in principal strain direction derived from data of Fig. 2

The paint, which was sprayed as a background to highlight the painted grid lines, acted as a brittle coating in this test. The presence of large axial strains preceding the propagating crack tip and the alignment of the principal strain direction with the axial direction of the crack in the region of the crack tip was graphically demonstrated by the brittle coating crack pattern in Figure 4 where the crack arrested in the ungrooved section of the pipe.

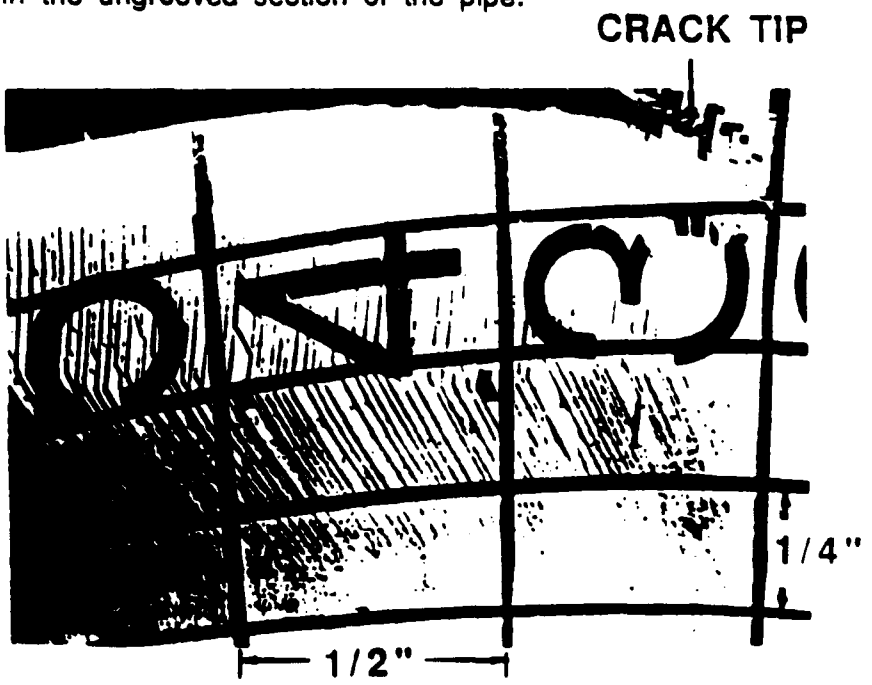

Figure 4. Brittle coating cracking pattern along crack path

Figure 4 shows the axial principal strain orientation and the region of large straining which extended on both sides of the crack path and at least one inch ahead of the crack tip.

The strain at the loci of the crack ends of the brittle coating pattern, i.e., along the isoentatics, is estimated to be larger than two percent. Also to be noted is the change in the direction of the cracking pattern approximately 1/2 in. away from the axial crack path in the upstream region. The 30° change in crack pattern indicates that the principal strain direction abruptly rotated upstream of the crack tip with the opening and stretching of the flaps and is consistent with Freund's shell model of axial pipe fracture [11].

The width of the brittle coating crack pattern and the lengthening of the painted grid lines indicated that a large axial plastic straining occurred in a narrow region surrounding the crack tip. The brittle coating pattern thus provided a qualitative confirmation of the strain gage measurements and its direction as well as the axial stretch model of the pipe flaps.

The CTOA of a crack, which ran out of the groove and arrested in the ungrooved section, is almost triple that of a running crack. This large CTOA suggests that the crack flap motion continued unabated for a short duration after the crack had slowed to an arrest.

Dynamic Crack Curving and Branching

The function of a tear strap in a pressurized fuselage is not so much to arrest a propagating axial crack by reducing the circumferential stress in the crack path, but to deflect the crack in the circumferential direction. A larger opening generated by the deflected crack will then result in a controlled depressurization of the fuselage and hence eliminate the driving force.

The mechanics of elastic crack curving as well as crack branching was studied by one of the authors and his colleague under an ONR contract [13, 14]. The dynamic crack curving criterion, which is a dynamic extension of the static criterion by Streit and Finnie [15], postulates that the micro-cracks ahead of a crack tip dictates the direction of crack propagation. The crack curving criterion assumes that when the circumferential stress within a prescribed crack tip region attains a maximum value off the axis of a self-similar crack extension, crack curving will occur. This maximum condition, which is based on linear elastic fracture mechanics (LEFM), results in a characteristic crack tip distance, r_o, in which the propagating crack will deviate from its axis by an angle of θ_c. For a static crack, these values are

$$r_o = \frac{9}{128\pi}\left[\frac{K_I}{\sigma_{ox}}\right]^2$$

and the crack curving angle, θ_c, is

$$\theta_c = \cos^{-1}\left[\frac{1 \pm \sqrt{1+\frac{1024\pi}{9} r_c \left(\frac{\sigma_{ox}}{K_I}\right)^2}}{\frac{512\pi}{9} r_c \left(\frac{\sigma_{ox}}{K_I}\right)^2}\right]$$

where K_I and σ_{ox} are the mode I stress intensity factor and the remote stress component or the first nonsingular term in the elastic crack tip stress field, respectively. The elastic crack curving criterion requires that $r_o < r_c$ for the crack to curve an angle, θ_c, away from its axis where r_c is a material constant which specifies the characteristic crack tip region in which the off axis micro-cracks are triggered and connected to the main crack tip.

In the presence of a large driving force, or a large dynamic stress intensity factor, the crack will bifurcate in order to shed the excess driving force and thus results in crack branching while the crack branching angle is governed by the crack curving criterion. This crack branching criterion was used successfully to correlated the predicted and measured crack branching angle, $2\theta_c$, and the estimated crack branching stress intensity factor, K_{IB}, in a bursting steel pipe [16]

Finite Element Modeling of Axial Rupture of Aircraft Fuselage

Axial rupture of an aircraft fuselage differs significantly with the rupture of a line pipe in that the ratio of the half crack length, a, to the fuselage radius, R, is one to two orders of magnitude smaller than that of the line pipe. Also the crack flaps of the fuselage are initially loaded statically by the insulation, which acts as a bladder to maintain the cabin pressure on the flaps, and later by the aerodynamic windage as the flaps peel open. Figure 5 shows the axial and circumferential strain variations with crack extension from the static tests conducted in the DOT pipe rupture studies where the pipe pressure was maintained by a neoplene bladder reinforced by a Kevlar insert. The small flap openings in these tests, together with static pressure acting on the flaps simulated the initial phase of an axial rupture of a fuselage. As shown in Figure 5, the deforming flap in the static line pipe test also generated an axial strain which exceeds the circumferential strain at an distance approximately one half of the pipe radius ahead of the crack tip. This recurring theme in both the static and dynamic axial crack studies of the line pipe is the large axial strain which precedes the crack tip. This axial strain, which is three to five times larger than the circumferential strain, is the cause of crack curving once the propagating crack runs out of the groove in the line pipe.

In order to estimate the axial strain ahead of the crack tip in a rupturing aircraft, a finite element model of a two bay crack in an idealized fuselage, as shown in Figure 6, was studied. This quasi-static analysis accounts for the deforming flap geometry but ignores the stress wave effects. The quasi-static analysis was justified since the measure crack velocities in the DOT pipe rupture studies [7,8], full-scale steel pipe rupture studies [17] and dynamic fracture testing of single-edge notched, 7075-T6 and 7178-T6 aluminum specimens [18] all recorded crack velocities less than ten percent of the dilatational wave velocities.

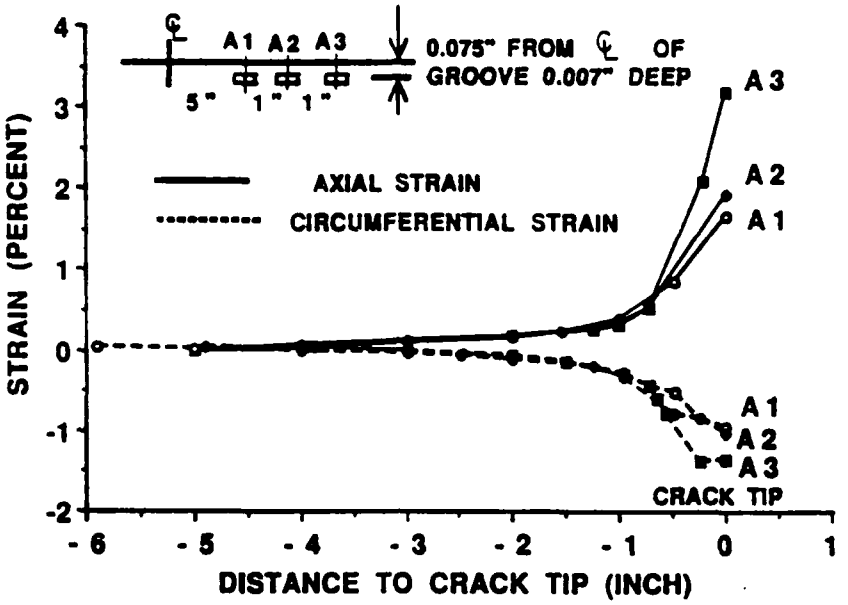

Fig. 5. Variations in strains. Crack length 16 in. Groove depth 0.007 in. Test No. S17.

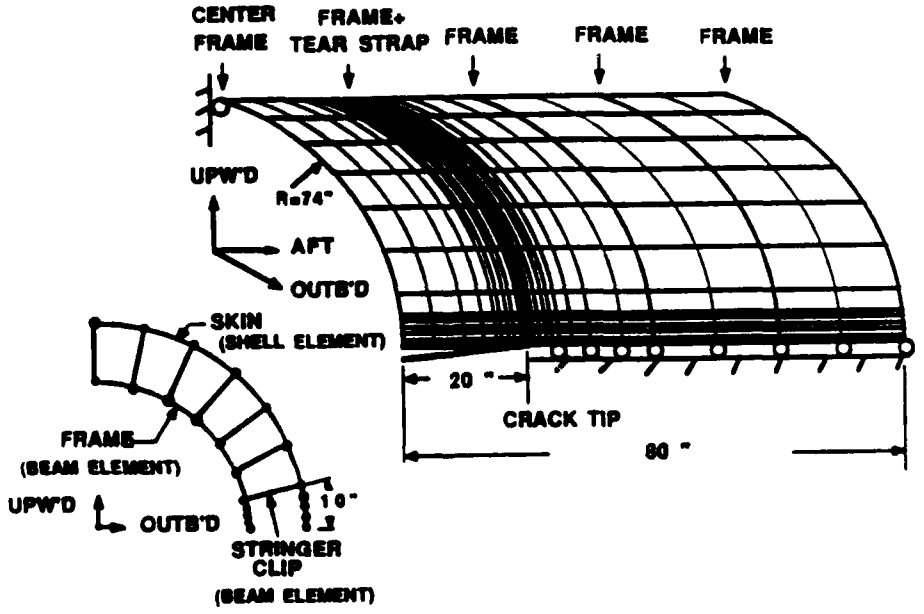

Fig. 6 Finite element model of an idealized fuselage with an axial crack

Table 1 shows some of the structural details and the material properties of the idealized fuselage considered in this study. The fuselage was assumed to be a pressurized cylindrical tube with an uniform axial tensile stress of pR/2t. While structural details, such as butt and overlap joints were ignored, the frame stiffness was incorporated by the beam elements as shown in Figure 6. Windage loading on the crack flaps was not considered due to the lack of measured pressure distribution on a fuselage flap of a moving airplane.

Parameter		Symbol	Value	Unit
Skin and Tear Strap	Material	2024-T3 Clad Sheet		
	Thickness	t	0.036	Inches
	Ultimate Strength	F_{tu}	62	ksi
	Yield Strength	F_{ty}	47	ksi
	Young's Modulus	E	10.5×10^3	ksi
	Fracture Toughness	Kc	91 *	ksi $\sqrt{in}$
	Fuselage Diameter	D	148	Inches
	Tear Strap Spacing	S	10	Inches
	Tear Strap Width	W	2	Inches
	Frame Spacing	b	20	Inches
	Crack Length	2a	40	Inches
	Limit Pressure Differential	P_{limit}	7.5	psi
	Fail-Safe Pressure Differential	P_{fs}	9.0	psi

* Ref. MCIC-HB-01R, "Damage Tolerant Design Handbook"

Table 1. Structural and material property data for aircraft fuselage analysis

Elastic and elastic-plastic static analyses, both based on large deformation shell theory, were conducted. Both analyses were conducted for a stationary axial crack of half crack length of a = 15 to 20 inches at one inch intervals. As such, this analysis does not account for the history of crack extension where the crack would grow from an initial crack length of the order of 1 in. to a = 15 - 20 inches. Thus the effect of the residual stresses in the unloaded crack flaps is also ignored. In all analyses, the center frame, as shown in Figure 7 was assumed to be intact and the riveted skin was assumed to have torn off 10 in. away from the crack. The results of this analysis is discussed in the following.

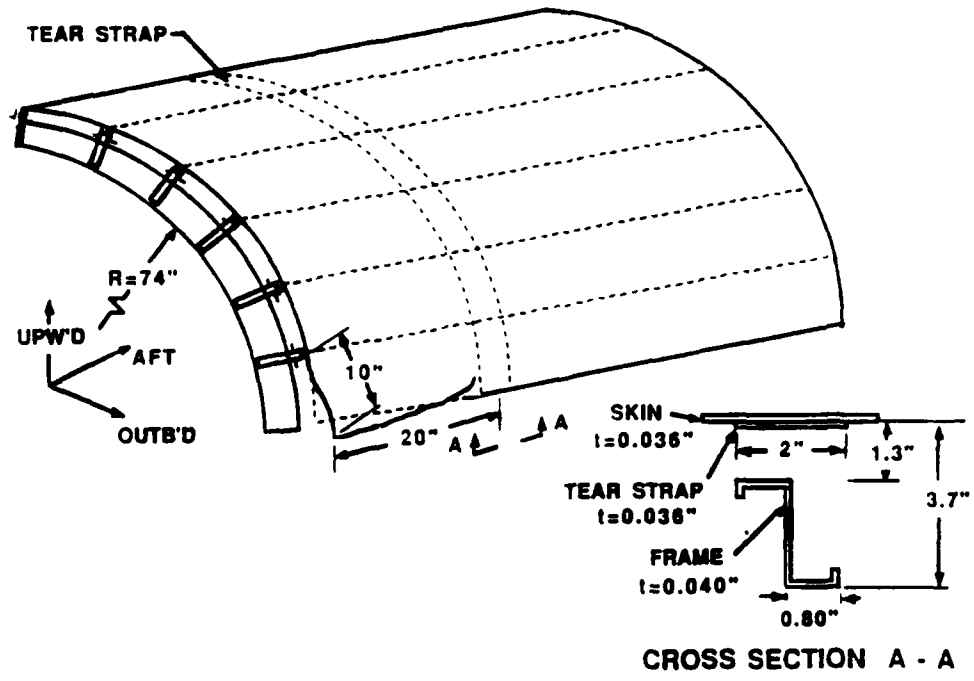

Fig. 7. Axial rupture of an idealized fuselage

Elastic Analysis

As the bursting pipe study showed, large plastic deformation precedes the propagating crack tip which is followed by extensive plastic unloading along the edges of the flaps. Although the elastic analysis in this section does not model the actual flap deformation process accurately, this zeroth order approximation provides an insight to the problem at hand.

Figure 8 shows the elastic stress distribution in a cracked fuselage, which is pressurized to a gage pressure of 7.5 psi and an axial tensile stress of 7.7 ksi, with a crack length of a = 16 in. The numbers with an asterisk are the computed axial stresses in each finite element. The lower numbers represent the axial to circumferential stress ratios. The coarse finite element mesh of Figure 6 was calibrated against a known solution, i.e. a central crack in an infinite plate under uniaxial tension in this case, such that the stress intensity factor and the remote stress component, σ_{ox}, could be extracted from the circumferential and axial stresses at the center of the forward crack tip element. This calibration scheme was essential for extracting meaningful fracture data from the coarse grid finite element analysis.

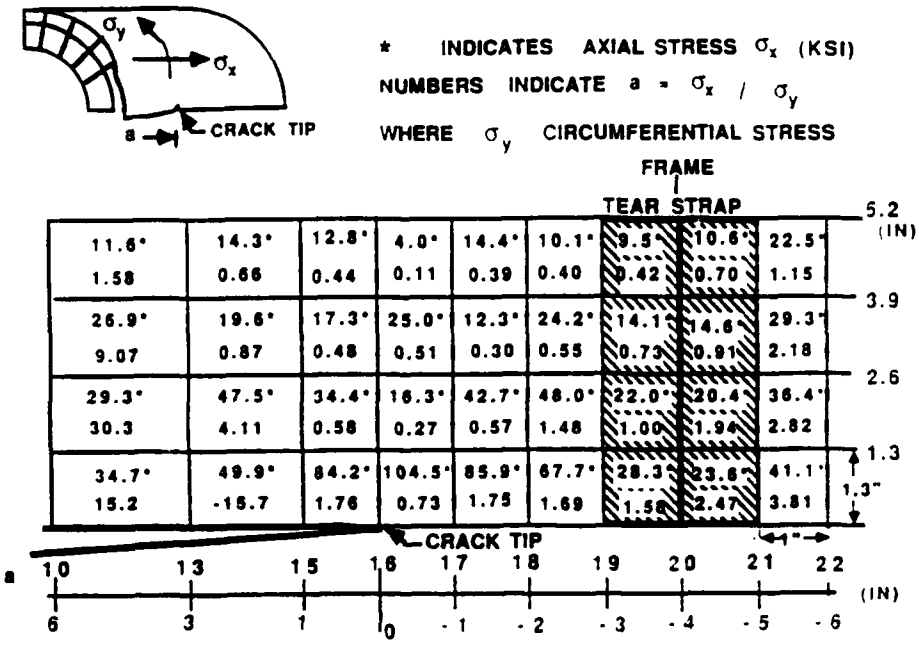

Fig. 8. Elastic stress distribution in a cracked pressurized fuselage

Table 2 shows the mode I stress intensity factor, K, and the characteristic distance, r_o, for half crack lengths ranging from a = 15 through 20 in. where the crack was assumed to have penetrated halfway through the tear strap. Also shown is the crack curving angle, θ_c, which was predicted by using the crack curving criterion as described in the previous section, for these crack lengths. The critical material property for crack curving, r_c, was assumed to be 1.0 ~ 1.5 mm following similar analysis for steel pipes [16]. Note that the high axial stress for

p (psi)	a (in)	K (ksi$\sqrt{in}$)	σ_{ox} (ksi)	r_o (mm)	θ_c (deg) r_c =1mm	θ_c (deg) r_c =1.5mm
	15	144.	73.0	2.2	-	-
	16	149.	88.3	1.6	-	-
4.5	17	151.	109.	1.1	-	35.6
	18	157.	130.	0.8	27.6	46.9
	19	110.	52.3	2.5	-	-
	20	113.	62.3	1.9	-	-
	15	220.	98.0	2.9	-	-
	16	225.	120.	2.0	-	-
7.5	17	228.	148.	1.3	-	21.8
	18	235.	178.	1.0	2.8	40.0
	19	166.	68.2	3.4	-	-
	20	172.	79.5	2.7	-	-

Table 2. Results of elastic analysis

much of the crack length, a, would have caused the crack to curve if the fuselage was not weakened by stress concentrations and multiple site damages along its path. Thus, similar to the 2-in. pipe rupture tests, the axial crack in the fuselage propagated straight ahead only in the presence of the MSD's which acted as a crack guide.

Exception to the tendency for crack curving can be seen in longest crack which was assumed to have penetrated into the tear strap. In this case, $r_o > r_c$ and the necessary condition for crack curving is violated, thus suggesting that the crack will propagate axially once it has fractured the tear strap.

Elastic-Plastic Analysis

Figures 9, 10 and 11 show the axial stresses and the axial-to-circumferential stress ratios in the finite elements surrounding the crack tip for half crack length of a = 15, 18 and 20 in. Figures 9 and 10 represent the states of crack tip stress as the crack approaches the tear strap and Figure 11 represents the state of stress when the crack penetrated the tear strap. Note that the axial-to-circumferential stress ratio exceeds unity for a = 18 in. and is a low 0.6 when the crack had penetrated the tear strap.

The crack curving and crack branching criteria described above obviously is not applicable to the elastic-plastic states of stress of Figures 9, 10 and 11. If, however, the state of stress governs the fracture process, then the crack curving and crack branching criteria can be used to estimate the onset of crack curving as well as the crack curving angle. The rational for using such crude approximation is analogous to the use of plasticity corrected stress intensity factor in LEFM.

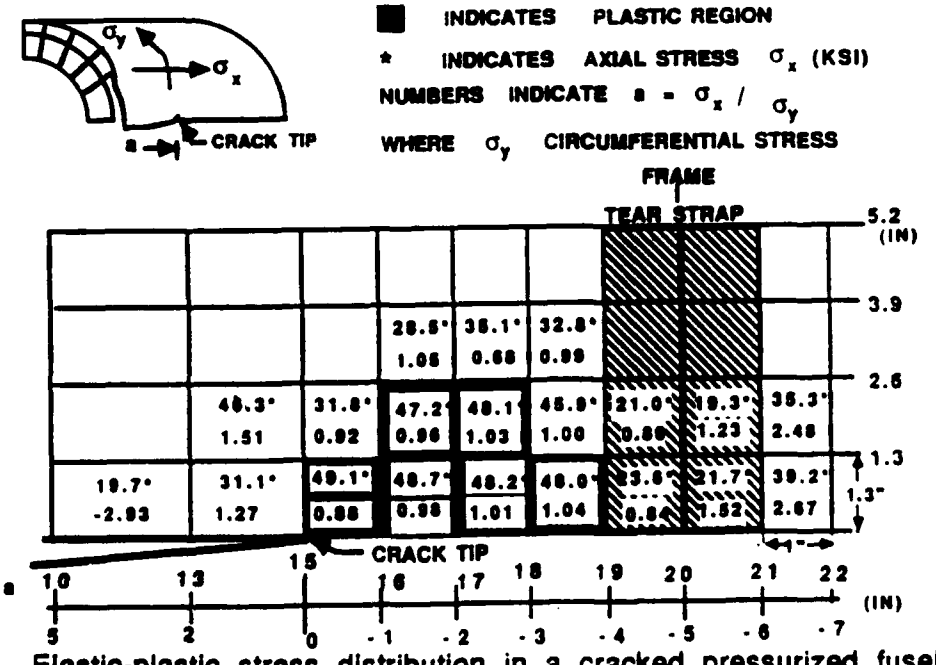

Fig. 9. Elastic-plastic stress distribution in a cracked pressurized fuselage

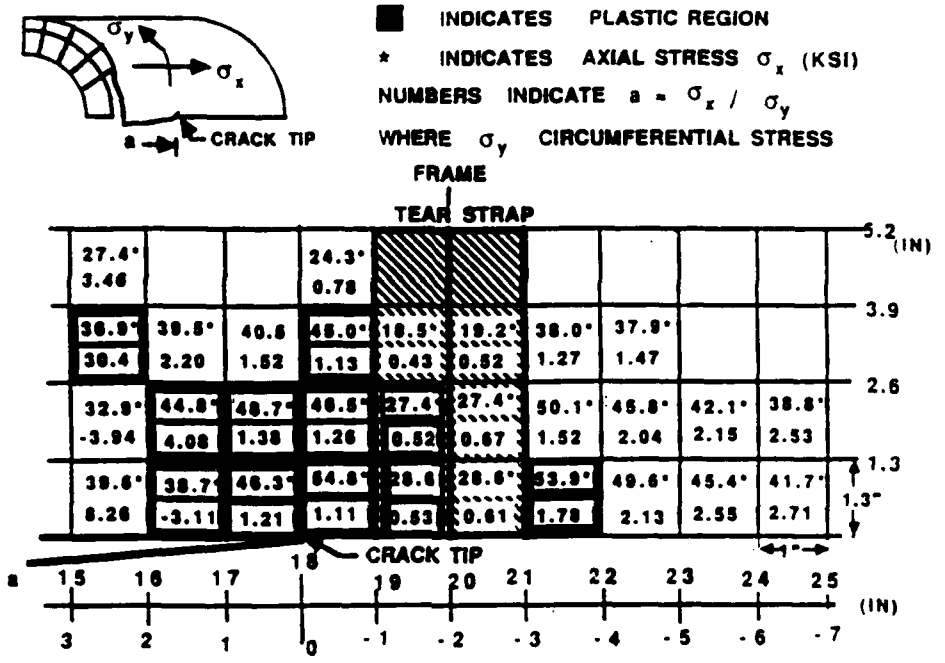

Fig. 10. Elastic-plastic stress distribution in a cracked pressurized fuselage

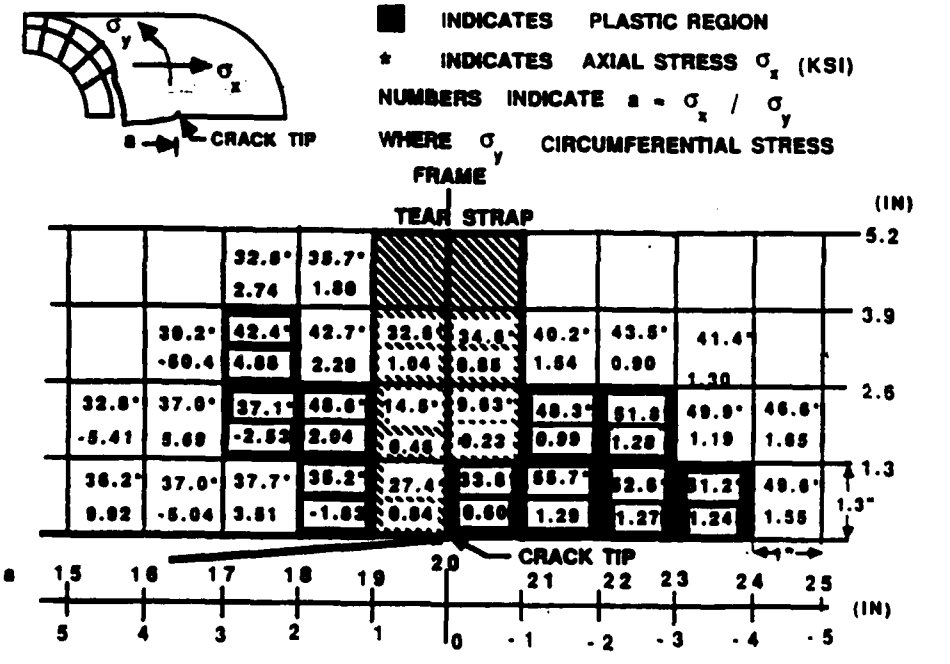

Fig. 11. Elastic-plastic stress distribution in a cracked pressurized fuselage

Table 3 shows the plasticity corrected mode I stress intensity factor, K, the remote stress component, σ_{ox}, the characteristic distance, r_o, and the crack curving angle, θ_c for two fuselage pressures of p = 4.5 and 7.5 psi. The results show that crack curving is inevitable in the skin before the crack arrived at the tear strap.

p (psi)	a (in)	K (ksi$\sqrt{in}$)	σ_{ox} (ksi)	r_o (mm)	θ_c (deg) r_c =1mm	θ_c (deg) r_c =1.5mm
4.5	15	75.5	62	0.8	26.7	46.5
	16	78.1	62	0.9	20.9	44.0
	17	79.2	62	0.9	17.9	42.9
	18	73.0	62	0.8	31.2	48.7
	19	85.3	28.4	5.1	-	-
	20	83.9	39.1	2.6	-	-
7.5	15	86.2	61.7	1.1	-	34.9
	16	88.3	62	1.1	-	32.7
	17	85.2	62	1.1	-	36.6
	18	78.5	62	0.9	19.9	43.6
	19	90.2	24.7	7.6	-	-
	20	90.8	36.6	3.5	-	-

Table 3. Results of elastic-plastic analysis

The fuselage in this analysis is a shell of uniform thickness without rivets. The stress concentrations at the row of rivet holes in the actual fuselage will locally increase the circumferential stress and simulate the groove in the line-pipe experiment. Thus an axial crack in the actual fuselage will continue to propagate axially, particularly in the presence of a multiple site damage. As the axial crack in such damaged fuselage approaches the tear strap, however, crack curving is inevitable if the integrity of the tear strap is maintained as shown by Figure 10. If the axial crack penetrates the tear strap, as shown in Figure 11, then it will continue to propagate axially without curving through the tear strap.

Conclusions

Large deformation elastic-plastic finite element analysis of a pressurized fuselage showed that a large axial stress component exists ahead of an axial crack. The computed crack tip stress, when combined with a previously developed crack curving criterion, predicted crack curving throughout much of the skin.

Discussions

The numerical analysis and results presented in this paper should be considered a first order approximation to the complex state of stress in an actual fuselage. The analysis could be easily upgraded by incorporating the history effect of plastic deformation by incrementally advancing the axial crack tip.

A more difficult task is to develop a crack curving and crack branching criteria in the presence of large plastic deformation. If, for example, a maximum strain criterion is used for crack curving, then crack curving will not occur until the crack tip is close to the tear strap as indicated by the axial-to-circumferential stress ratios in Figures 9, 10 and 11.

Acknowledgement

The results on axial cracking of line-pipe was obtained under DOT contract DTRS - 5683-C-0009. The results on crack curving and crack branching as well as the analysis reported in this paper was obtained under the sponsorship of ONR contract N00014-89-J-1276. The authors wish to express their gratitude to Dr. Y. Rajapakse for his continuous support of this investigation.

References

1. Folias, E.S.; A Finite Line Crack in a Pressurized Cylindrical Shell. Intl. J. of Fracture Mechanics. 1 (Jun. 1965) 104-113.

2. Erdogan, F.; Kibler, J.J.; Cylindrical and Spherical Shells with Cracks. Intl. J. of Fracture Mechanics. 5 (Sept. 1969) 229-236.

3. Ramulu, M.; Kobayashi, A.S.; Kang, B.S.-J.; Dynamic Crack Curving and Branching in Line-Pipe. ASME J. of Pressure Vessel Technology. 104 (1982) 317-322.

4. Hahn, G.T.; Sarrate, M.; Rosenfield, A.R.; Criteria for Crack Extension in Cylindrical Pressure Vessels. Intl. J. of Fracture Mechanics. 5 (1969) 187-210.

5. Maxey, W.A.; Dynamic Crack Propagation in Line Pipe. Proc. of Intl. Conf. on Analytical and Experimental Fracture Mechanics. Sijthoff and Noordhoff (1980) 109-223.

6. Freund, L.B.; Parks, D.M.; Analytical Interpretation of Running Ductile Fracture Experiments in Gas Pressurized Linepipe. Crack Arrest Methodology and Applications. Hahn/Kanninen eds. ASTM STP 711 (1980) 359-378.

7. Kobayashi, A.S.; Emery, A.F.; Love, W.J.; Chao, Y.H.; Johannson, O.; Crack Bifurcation and Arrest in Pressurized Pipe. Fracture Mechanics: Nineteenth Symposium. ASTM STP 969 (1988) 441-465.

8. Kobayashi, A.S.; Emery, A.F.; Love, W.J.; Chao, Y.H.; Subsize Experiments and Numerical Modelling of Axial Rupture of Gas Transmission Lines. ASME Pressure Vessel Technology. 110 (May 1988) 155-160.

9. Shoemaker, A.K.; McCartney, R.F.; Displacement Consideration for a Ductile Propagating Fracture in a Line Pipe. ASME Journal of Engineering Materials Technology. 96 ((1974) 318-322.

10. Urednicek, M.; Control of Ductile Fracture Propagation in Large Diameter Gas Transmission Pipelines. ASME Winter Annual Meeting Preprint. 83-WA/PVP-11 (November 1983).

11. Freund, L.G.; Parks, D.M.; Rice, J.R.; Running Ductile Fracture in a Pressurized line Pipe. Mechanics of Crack Growth. ASTM STP 590 (1976) 243-262.

12. Freund, L.B.; Li, V.C.F.; Parks, D.M.; An Analysis of a Wire-Wrapped Mechanical Crack Arrester for Pressurized Pipelines. ASME J. of Pressure Vessel Technology. 101 (Feb. 1979) 51-58.

13. Ramulu, M.; Kobayashi, A.S.; Dynamic Crack Curving - A Photoelastic Evaluation. Experimental Mechanics. 23 (March 1983) 1-9.

14. Ramulu, M.; Kobayashi, A.S.; Kang, B.S.-J.; Dynamic Crack Branching - A Photoelastic Evaluation. Fracture Mechanics: Fifteen Symposium. Ed. by R. J. Sanford. ASTM STP 833 (1984) 130-148.

15. Streit, R: Finnie, I.; An Experimental Investigation of crack Path Directional Stability. Experimental Mechanics. 20 (January 1980) 17-23.

16. Ramulu, M.; Kobayashi, A.S.; Kang, B.S.-J.; Dynamic Crack Curving and Branching in Line-Pipe. ASME Journal of Pressure Vessel Technology. 104 (November 1982) 317-322.

17. Bromo, F.; Bramante, M.; Spedaletti, M.; Ductile Fracture Propagation in Pipelines: Results of Instrumented Full-Scale Burst Tests on 48" and 56" Diametral Pipes for gas Transmission. Analytical and Experimental Fracture Mechanics. G.C. Sih and M. Mirahik eds. Sijthoff and Noordhoff (1980) 567-578.

18. Kobayashi, A.S.; Engstrom, W.L.; Transient Analysis in Fracturing Aluminum Plate. Proc. of JSME 1967 Semi-International Symposium (1987) 172-182.

ASK/cm

Office of Naval Research
800 N Quincy Street
Arlington, VA 22217-5000
Attn: Code 11325M (4 copies)

Office of Naval Research
800 N Quincy Street
Arlington, VA 22217-5000
Attn: Code 1131

Defense Documentation Cntr
(4 copies)
Cameron Station
Alexandria, VA 02314

Naval Research Laboratory
Washington, DC 20375
Attn: Code 6000

Naval Research Laboratory
Washington, DC 20375
Attn: Code 6300

Naval Research Laboratory
Washington, DC 20375
Attn: Code 6380

Naval Research Laboratory
Washington, DC 20375
Attn: Code 5830

Naval Research Laboratory
Washington, DC 20375
Attn: Code 6390

Naval Research Laboratory
Washington, DC 20375
Attn: Code 2620

David W. Taylor Naval Ship
R & D Center
Annapolis, MD 21402
Attn: Code 28

David W. Taylor Naval Ship
R & D Center
Annapolis, MD 21402
Attn: Code 2812

David W. Taylor Naval Ship
R & D Center
Annapolis, MD 21402
Attn: Code 2814

David W. Taylor Naval Ship
R & D Center
Annapolis, MD 21402
Attn: Code 1700

David W. Taylor Naval Ship
R & D Center
Annapolis, MD 21402
Attn: Code 1720

David W. Taylor Naval Ship
R & D Center
Annapolis, MD 21402
Attn: Code 1720.4

Naval Air Development
Center
Warminster, PA 18974
Attn: Code 6043

Naval Air Development
Center
Warminster, PA 18974
Attn: Code 6063

Naval Surface Weapons
Center
White Oak, MD 20910
Attn: Code R30
Technical Library

Naval Surface Weapons
Center
Dahlgren, VA 22448
Attn: Technical Library

Naval Civil Eng Library
Port Hueneme, CA 93043
Attn: Technical Library

Naval Underwater Systems
Center
New London, CT 06320
Attn: Code 44
Technical Library

Naval Underwater Systems
Center
Newport, RI 02841
Attn: Technical Library

Naval Weapons Center
China Lake, CA 99555
Attn: Technical Library

NRL/Underwater Sound
Reference Dept.
Orlando, FL 32856
Attn: Technical Library

Chief of Naval Operations
Department of the Navy
Washington, DC 20350
Attn: Code OP-098

Commander
Naval Sea Systems Command
Washington, DC 20362
Attn: Code 05R25

Commander
Naval Sea Systems Command
Washington, DC 20362
Attn: Code 05R26

Commander
Naval Sea Systems Command
Washington, DC 20362
Attn: Code 09B31

Commander
Naval Sea Systems Command
Washington, DC 20362
Attn: Code 55Y

Commander
Naval Sea Systems Command
Washington, DC 20362
Attn: Code 55Y2

Commander
Naval Sea Systems Command
Washington, DC 20362
Attn: Code 03D

Commander
Naval Sea Systems Command
Washington, DC 20362
Attn: Code 7226

Commander
Naval Sea Systems Command
Washington, DC 20362
Attn: Code 310A

Commander
Naval Sea Systems Command
Washington, DC 20362
Attn: Code 310B

US Naval Academy
Mechanical Engineering Dept.
Annapolis, MD 21402

Naval Postgraduate School
Monterey, CA 93940
Attn: Technical Library

Mr. Jerome Persh
Stf Specit for Matls &Struct
OUSDE & E. The Pentagon
Room 3D1089
Washington, DC 20301

Professor J. Hutchinson
Harvard University
Div. of Applied Sciences
Cambridge, MA 02138

Dr. Harold Liebowitz, Dean
School of Engr. & Applied Sci.
George Washington
University
Washington, DC 20052

Professor G.T. Hahn
Vanderbilt University
Dept. of Mech. & Matrls. Engr.
Nashville, TN 37235

Professor Albert S. Kobayashi
Dept. of Mechanical
Engineering
University of Washington
Seattle, WA 98195

Professor L.B. Freund
Brown University
Division of Engineering
Providence, RI 02912

Professor B. Budiansky
Harvard University
Division of Applied Sciences
Cambridge, MA 02138

Professor S.N. Atluri
Georgia Institute of
Technology
School of Engr. & Mechanics
Atlanta, GA 30332

Professor G.Springer
Stanford University
Dept. of Aeronautics
& Astronautics
Stanford, CA 94305

Professor H.T. Hahn
Washington University
Center for Composites
Research
St. Louis, MO 63130

Professor S.K. Datta
University of Colorado
Dept. of Mechanical
Engineering
Boulder, CO 80309

Dr. M.L. Williams
School of Engineering
University of Pittsburgh
Pittsburgh, PA 15261

Dr. D.C. Drucker
Dept. of Aerospace Eng. &
Mechanics
University of Florida
Tallahassee, FL 32611

Dean B.A. Boley
Dept. of Civil Engineering
Northwestern University
Evanston, IL 60201

Professor J. Duffy
Brown University
Division of Engineering
Providence, RI 02912

Professor J D Achenbach
Northwestern University
Dept of Civil Engineering
Evanston, IL 60208

Professor F A. McClintock
Dept of Mechanical
Engineering
Massachusetts Institute o
Technology
Cambridge, MA 02139

Professor D.M. Parks
Dept of Mechanical
Engineering
Massachusetts Institute o
Technology
Cambridge, MA 02139

Dr. M.F. Kanninen
Southwest Research Inst
PO Drawer 28510
6220 Culebra Road
San Antonio, TX 78284

Professor F.P. Chiang
Dept of Mechanical Engr
State U of NY at Stony Br
Stony Brook, NY 11794

Professor S.S. Wang
Dept of Theoretical & Ap
Mechs
University of Illinois
Urbana, IL 61801

Professor Y. Weitsman
Civil Engr Department
Texas A&M University
College Station, TX 7784

Professor I.M. Daniel
Dept of Mechanical Engr
Illinois Institute of
Technology
Chicago, IL 60616

Professor C.T. Sun
School of Aeronautics &
Astronautics
Purdue University
W. Lafayette, IN 47907

Professor J. Awerbuch
Dept of Mech Engr &
Mechanics
Drexel University
Philadelphia, PA 19104

Professor T.H. Lin
University of California
Civil Engineering Dept
Los Angeles, CA 90024

Professor G J Dvorak
Dept of Civil Engr
Rensselaer Polytecnic
Institute

UNCLASSIFIED

SECURITY CLASSIFICATION OF THIS PAGE (When Data Entered)

REPORT DOCUMENTATION PAGE		READ INSTRUCTIONS BEFORE COMPLETING FORM
1. REPORT NUMBER UWA/DME/TR-90/66	2. GOVT ACCESSION NO.	3. RECIPIENT'S CATALOG NUMBER
4. TITLE (and Subtitle) AXIAL CRACK PROPAGATION AND ARREST IN PRESSURIZED FUSELAGE		5. TYPE OF REPORT & PERIOD COVERED Technical Report 6. PERFORMING ORG. REPORT NUMBER UWA/DME/TR-90/66
7. AUTHOR(s) M. Kosai and A.S. Kobayashi		8. CONTRACT OR GRANT NUMBER(s) N00014-89-J-1276
9. PERFORMING ORGANIZATION NAME AND ADDRESS Department of Mechanical Engineering, FU-10 University of Washington, Seattle, WA 98195		10. PROGRAM ELEMENT, PROJECT, TASK AREA & WORK UNIT NUMBERS
11. CONTROLLING OFFICE NAME AND ADDRESS Office of the Chief of Naval Research Arlington, VA 22217-5000		12. REPORT DATE April 1990 13. NUMBER OF PAGES 15
14. MONITORING AGENCY NAME & ADDRESS(if different from Controlling Office)		15. SECURITY CLASS. (of this report) Unclassified 15a. DECLASSIFICATION/DOWNGRADING SCHEDULE

16. DISTRIBUTION STATEMENT (of this Report)

Unlimited

17. DISTRIBUTION STATEMENT (of the abstract entered in Block 20, if different from Report)

18. SUPPLEMENTARY NOTES

19. KEY WORDS (Continue on reverse side if necessary and identify by block number)

Dynamic fracture, crack arrest, pressurized fuselage, tear straps.

20. ABSTRACT (Continue on reverse side if necessary and identify by block number)

The rapid crack propagation, crack curving and arrest mechanisms associated with a pressurized, thin-walled ductile steel tubes are used to develop a model of axial rupture of an aircraft fuselage. This model is used to replicate axial crack propagation along a line of multi-site damage (MSD) and crack curving and arrest near a tear strap of an idealized fuselage.

DD FORM 1 JAN 73 1473 EDITION OF 1 NOV 65 IS OBSOLETE
S/N 0102-014-6601

UNCLASSIFIED

SECURITY CLASSIFICATION OF THIS PAGE (When Data Entered)

90 05 09 16